Plasticization Effects on Bubble Growth During Polymer Foaming

Xiaopeng Chen, James J. Feng,
Department of Chemical and Biological Engineering and Department of Mathematics, University of British Columbia, Vancouver, Canada V6T 1Z3

Christopher A. Bertelo
Arkema Research Center, 900 First Avenue, King of Prussia, Pennsylvania 19406

During polymer foaming with physical blowing agents, plasticization affects the melt viscosity, gas diffusivity in the melt, and the gas–melt interfacial tension. In this paper, we propose a model for plasticization during bubble growth, and estimate its effects under typical foaming conditions. The theoretical model incorporates well-established mixture theories into a recent model for diffusion-induced bubble growth. These include the free-volume theories for the viscosity and diffusivity in polymer-blowing agent mixtures and the density gradient theory for the interfacial tension. The viscoelasticity of the melt is represented by an Oldroyd-B constitutive equation. We study the radial growth of a single bubble in an infinite expanse of melt, using parameter values based on experiments on polystyrene–CO_2 systems. Our results show that even at relatively low gas concentrations, plasticization increases the blowing-agent diffusivity markedly and thus boosts the rate of bubble growth. In contrast, the reduction in melt viscosity and interfacial tension has little effect on bubble growth. Though not intended as quantitative guidelines for process design, these results are expected to apply qualitatively to typical foaming conditions and common polymer-blowing agent combinations. POLYM. ENG. SCI., 46: 97–107, 2006. © 2005 Society of Plastics Engineers

INTRODUCTION

The foaming of polymer melts has been studied by many authors, both theoretically [e.g., 1–8] and experimentally [e.g., 9–12]. Extensive reviews and references can be found in a handbook edited by Klempner and Frisch [13] and a monograph by Lee [14]. From a modeling point of view, the process can be divided into three stages: bubble nucleation, bubble growth, and possibly coarsening. Bubble growth is perhaps the most thoroughly studied of the three, with models incorporating gas diffusion, momentum transfer, melt viscoelasticity, and bubble–bubble interactions via a cell model [2, 7]. Shafi et al. [4] and Feng and Bertelo [8] further combined phenomenological nucleation models with single-bubble growth models to predict the final cell size distribution. In such studies, all material properties are treated as constants. In reality, however, they vary as a result of changing temperature and solvent concentration. The dependence of material properties on solvent concentration is the focus of this paper.

Plasticization refers to the change in melt properties due to small-molecule solvents in the polymer. Deplasticization is the reverse process when the solvent is removed from the melt. In the context of polymer foaming, plasticization takes place when a physical blowing agent is dissolved into the melt under pressure, whereas deplasticization occurs when, upon release of the pressure or elevation of temperature, the blowing agent separates from the melt and aggregates into gas bubbles. This paper is concerned with both processes, and we use the term plasticization generally to refer to the dependence of the properties of the polymer–gas mixture on gas concentration. In particular, plasticization affects three properties that are potentially significant to foaming. (i) Viscosity μ: When a blowing agent is dissolved, the polymer melt typically experiences a drastic reduction in viscosity. Conversely, as the gas concentration c drops during foaming, the viscosity recovers. (ii) Gas diffusivity D: The dissolved gas will modify the molecular environment for its diffusion through the polymer during foaming, typically raising the gas diffusivity. (iii) Gas–polymer interfacial tension σ: The interfacial tension reflects the interaction between the two species of molecules, which will be influenced by the presence of the blowing agent molecules in the melt.

Correspondence to: James J. Feng; e-mail: jfeng@chml.ubc.ca
Contract grant sponsor: Arkema Inc., Canada; contract grant sponsor: NSERC, Canada; contract grant sponsor: NSF, U.S.A.; contract grant numbers: CTS-0229298, CTS-9984402; contract grant sponsor: NNSF, China; contract grant numbers: 20174024, 20490220.
DOI 10.1002/pen.20434
Published online in Wiley InterScience (www.interscience.wiley.com).

All three factors directly affect the growth of gas bubbles, and therefore may have an impact on the bubble-size distribution and ultimate properties of the foam product. Yet, relatively little information is available in the literature. Gendron et al. [15] described an experimental study of plasticization of polystyrene (PS) by the blowing agents HCFC 142b and HFC 134a. The melt viscosity is shown to decrease by 2 orders of magnitude for gas concentration up to 15%. Two possible mechanisms have been considered for this reduction in viscosity: an increase in free volume (FV) or a simple dilution effect. The William–Landel–Ferry (WLF) equation (see *Eq. 14*) can be fitted to the data, although the fitting parameters need to be adjusted at different temperatures. Ramesh and Malwitz [16] reported much smaller viscosity reduction (about 50%) in low-density polyethylene (LDPE) melts with a blowing agent concentration up to 20%. The data were fitted to a $\mu(c)$ correlation that, together with a $D(c)$ correlation from data on butane in LDPE, was used to calculate bubble growth in a concentric cell model. Finally, Lee and Flumerfelt [17] developed a model for the change in the gas–polymer interfacial tension σ based on the energy of molecular interactions. The model can be tuned to fit experimental data on LDPE–N_2 systems, which show a nearly 50% reduction in σ at a saturation concentration of about 1.84 wt% N_2.

The objective of this paper is to assess the effect of plasticization on polymer foaming. This is done by integrating well-established theories for the viscosity, diffusivity, and interfacial energy of fluid mixtures to the model of Feng and Bertelo [8] for diffusion-induced bubble growth in a viscoelastic melt. We have chosen to simulate the foaming experiment of Han and Yoo [9] for a PS–CO_2 system. Among experiments reported in the literature, this provides the most detailed description of the experimental conditions and results. Still, some physical parameters required by the mixture theories were not given. For these, we will have to adopt values in the literature for comparable materials. Besides, Han and Yoo's [9] experimental conditions are not necessarily representative of industrial foaming operations. For example, the CO_2 concentration of 0.2 wt% is much below commercial levels. Although solubility varies greatly among blowing agents, concentrations over 10 wt% are routinely used [15, 16]. For these reasons, we have not intended our model predictions to be quantitatively meaningful for process design. Rather, we will illuminate the fundamental physics that causes plasticization, establish the processing conditions under which it does or does not influences bubble growth, and provide estimates on the magnitude of the effects.

BUBBLE GROWTH MODEL

Diffusion-Induced Bubble Growth Without Plasticization

The model to be used in this work is based on Feng and Bertelo's simpler model [8] for diffusion-induced bubble growth without plasticization. In that model, a gaseous blowing agent is dissolved into a polymer melt under high pressure P_0 to saturation. Then the pressure is reduced to P_a suddenly, and the blowing agent becomes super-saturated and bubbles nucleate. A viable bubble proceeds to grow as the dissolved gas diffuses into the bubble. The isothermal growth of a spherical bubble in an infinite sea of melt is governed by the coupled processes of mass and momentum transport. The rheology of the polymer melt, represented by the Oldroyd-B model, contributes through the polymer stress as the melt undergoes biaxial extension. To make the governing equations dimensionless, we use the initial drop radius R_0 as the length scale and R_0^2/D as the time scale, where D is the constant diffusivity of the gas in the melt. Pressure and stresses are scaled by $\mu D/R_0^2$, where $\mu = \mu_s + \mu_p$ is the constant viscosity of the Oldroyd-B melt with solvent and polymer contributions. The gas concentration c is scaled by its initial value c_0. Then we can write the following dimensionless transport equations for mass and momentum and constitutive equations for the Oldroyd-B melt:

Momentum equation

$$P_g - P_a^* = Re\left(R\ddot{R} + \frac{3}{2}\dot{R}^2\right) + \frac{2}{Ca}\frac{1}{R} + \frac{4\beta\dot{R}}{\mathrm{R}} - 2\int_R^\infty \frac{\tau_{rr} - \tau_{\theta\theta}}{r}\,dr \quad (1)$$

Mass balance for gas in the bubble

$$\frac{d}{dt}(P_g R^3) = \frac{3}{A^* k^*} R^2 \frac{\partial c}{\partial r}\Big|_{r=R} \quad (2)$$

Mass balance for gas in melt

$$\frac{\partial c}{\partial t} + v\frac{\partial c}{\partial r} = \frac{1}{r^2}\frac{\partial}{\partial r}\left(r^2\frac{\partial c}{\partial r}\right) \quad (3)$$

Oldroyd-B constitutive equations

$$\tau_{rr} + De\left(\frac{d\tau_{rr}}{dt} + \frac{4R^2\dot{R}}{r^3}\tau_{rr}\right) = -4(1-\beta)\frac{R^2\dot{R}}{r^3} \quad (4)$$

$$\tau_{\theta\theta} + De\left(\frac{d\tau_{\theta\theta}}{dt} - \frac{2R^2\dot{R}}{r^3}\tau_{\theta\theta}\right) = 2(1-\beta)\frac{R^2\dot{R}}{r^3} \quad (5)$$

where the dot above R indicates time derivative, and the radial velocity $v = R^2\dot{R}/r^2$. The five unknowns are the bubble pressure $P_g(t)$, the bubble radius $R(t)$, the mass concentration of the blowing agent inside the melt $c(r,t)$, and the two polymer stress components $\tau_{rr}(r,t)$ and $\tau_{\theta\theta}(r,t)$. The dimensionless parameters are defined as [8]: $P_a^* = P_a R_0^2/(\mu D)$, P_a being the constant ambient pressure; the diffusion Reynolds number $Re = \rho D/\mu$; the capillary number $Ca = \mu D/\sigma R_0$, σ being a constant interfacial tension; β

DOI 10.1002/pen

$= \mu_s/\mu$; $k^* = k\mu D/c_0 R_0^2$, k being the Henry's law constant; $A^* = A/k$, A being the ratio between gas density and pressure inside the bubble; and the Deborah number $De = \lambda D/R_0^2$, λ being the polymer relaxation time. These equations are supplemented by the following initial and boundary conditions: $c(r,0) = 1$, $c(\dot{R},t) = k^* P_g(t)$ (Henry's law), $c(\infty,t) = 1$, $R(0) = 1$, $\dot{R}(0) = 0$, $P_g(0) = P_a^* + 2/Ca$, $\tau_{rr}(r,0) = \tau_{\theta\theta}(r,0) = 0$.

Diffusion-Induced Bubble Growth With Plasticization

Equations 1–5 are based on constant physical properties. As the bubble starts to grow, the gas concentration outside the bubble drops, and a radial $c(r)$ profile develops. In real materials, this will imply spatial profiles of the viscosity and gas diffusivity, which also evolve in time. Together with a changing interfacial tension, these enter the mass and momentum transfer and modify the growth rate of the bubble. We will introduce plasticization effects by making these three properties dependent on the gas concentration: polymer viscosity $\tilde{\mu}_p(\tilde{c})$, blowing agent diffusivity $\tilde{D}(\tilde{c})$, and interfacial tension $\tilde{\sigma}(\tilde{c})$. The tilde indicates dimensional quantities. We will use their values at $\tilde{c}=0$ (i.e., for pure polymer) in nondimensionalizing the equations. The plasticization effects are then represented by ratios such as $D = \tilde{D}(\tilde{c})/\tilde{D}(0)$. Now the governing equations, in dimensionless form, are as follows:

$$P_g - P_a = Re\left(R\ddot{R} + \frac{3}{2}\dot{R}^2\right) + \frac{2\sigma}{Ca}\frac{1}{R} + \frac{4\beta\dot{R}}{R} - 2\int_R^\infty \frac{\tau_{rr}-\tau_{\theta\theta}}{r}dr, \quad \text{with } \sigma(c)=\tilde{\sigma}(\tilde{c})/\tilde{\sigma}(0) \tag{6}$$

$$\frac{d}{dt}(P_g R^3) = \frac{3D}{A^* k^*} R^2 \frac{\partial c}{\partial r}\Big|_{r=R} \tag{7}$$

$$\frac{\partial c}{\partial t} + v\frac{\partial c}{\partial r} = \frac{1}{r^2}\frac{\partial}{\partial r}\left(Dr^2\frac{\partial c}{\partial r}\right), \text{ with } D(c)=\tilde{D}(\tilde{c})/\tilde{D}(0) \tag{8}$$

$$\tau_{rr} + De\left(\frac{d\tau_{rr}}{dt} + \frac{4R^2\dot{R}}{r^3}\tau_{rr}\right) = -4(1-\beta)\mu\frac{R^2\dot{R}}{r^3}, \quad \text{with } \mu(c)=\tilde{\mu}(\tilde{c})/\tilde{\mu}(0) \tag{9}$$

$$\tau_{\theta\theta} + De\left(\frac{d\tau_{\theta\theta}}{dt} - \frac{2R^2\dot{R}}{r^3}\tau_{\theta\theta}\right) = 2(1-\beta)\mu\frac{R^2\dot{R}}{r^3}. \tag{10}$$

The initial and boundary conditions are the same as those for constant material constants.

The c-dependent coefficients μ, D, and σ do not change the structure of the equations, and we use the same method of lines as in Feng and Bertelo [8] for their numerical solution. Briefly, we transform the radial domain from $[R,\infty)$ to [0,1], and adopt a nonuniform grid with denser grid points near the bubble's surface. The diffusion and constitutive equations are discretized on this grid and the resulting system of ordinary differential equations is solved implicitly in time. Grid refinement and time step refinement have been carried out to ensure convergence of the results. Feng and Bertelo [8] have presented benchmark calculations validating the numerical algorithm.

VARIABLE VISCOSITY EFFECT

The Free Volume Model

The most widely used model for viscosity-reduction of polymers by a dissolved small-molecule "solvent" is the free volume (FV) model, based on a monomeric friction coefficient that varies with the exponential of the fractional FV [e.g., 15, 18]. This model in general fits experimental data quite well. Although some researchers argued that the FV model might not be suitable for molten polymers when the temperature is too high above the glass transition temperature T_g, evidence suggests that the FV effect will be dominant when the melt temperature is below $T_g + T_c$, with the temperature margin T_c typically around 100°C.

The free volume V_F is the difference between the real volume V_0 of a polymer melt or solution and the "occupied volume" of the molecules [19]. Doolittle [20] proposed an empirical equation for the viscosity in term of FV:

$$\eta = A\exp\left(B\frac{V_0}{V_F}\right) = A\exp(B/f) \tag{11}$$

where A and B are constants and f is the FV fraction. Cohen and Turnbull [21] provided a physical justification of this equation on the basis of molecular transport in the fluid. They assumed that the movement of molecules occurs where there is a nearby cage larger than some critical value. Under the assumption that no energy is needed for redistribution of FV at a constant volume, the self-diffusion coefficient D can be derived as

$$D = ga^*u\exp(-\gamma v^*/V_F) \tag{12}$$

where g is a geometric factor, a^* is roughly the diameter of the cage with a molecule in it, u is the molecular velocity that is proportional to the square root of temperature $T^{1/2}$, γ is a parameter to correct for overlap of FV, and v^* is the minimum void volume that permit a molecule to jump in, which is close to the molecular volume. Since the molecular diffusion is directly related to translational friction and the viscosity of material, *Eqs. 11* and *12* are equivalent.

On the basis of the Doolittle's model, the most popular version of FV viscosity theory is the WLF equation [19]. When the liquid temperature is above T_g, the dependence of the FV on temperature can be written as

$$f = f_g + \alpha_f(T - T_g) \tag{13}$$

where f_g is the FV fraction at T_g, and α_f is the thermal expansion coefficient of the FV. Substituting *Eq. 13* into *Eq. 11*, we get the WLF equation,

$$\log(\eta/\eta_g) = -\frac{c_1(T-T_g)}{c_2+T-T_g} \tag{14}$$

where the parameters c_1 and c_2 are practically independent of the solvent fraction for concentrated solutions [19]. T_g is the sole parameter reflecting the compositions of the mixture.

By assuming the same entropy for the pure polymer and its dilution in glassy state, Chow [22] successfully predicted T_g for 13 kinds of dilutions in PS, using the following model:

$$\ln\left(\frac{T_g}{T_{g0}}\right) = \psi[(1-\theta)\ln(1-\theta)+\theta\ln\theta] \tag{15}$$

$$\theta = \frac{\omega/\mathrm{MW}_1}{z(1-\omega)/\mathrm{MW}_2} \tag{16}$$

$$\psi = \frac{zR}{\mathrm{MW}_2\Delta C_p} \tag{17}$$

where T_{g0} is the glass transition temperature for the pure polymer and T_g for the solution whose weight fraction of diluent is ω. MW_1 and MW_2 are solvent and polymer molecular weights, respectively. ΔC_p is the change in specific heat of the polymer at its glass transition temperature, and R is the gas constant. The coordination number z is the number of possible neighboring sites around a monomer that permit other molecules or monomers to fit in. A value of $z = 2$ is found appropriate for mixtures of PS with a variety of diluents, and we will use $z = 2$ in our calculations. *Equations 14–17* allow the calculation of the viscosity of a diluted polymer melt $\mu(c)$ in our bubble growth model (*Eqs. 9 and 10*).

Bubble Growth With Variable Viscosity

Because the unique properties of CO_2 as a solvent for polymers [23], much research has been devoted to the plasticization effects of CO_2 on various polymers [24, 25].

TABLE 1. Parameter values for the WLF-Chow model as determined by Royer et al. [26] for CO_2 in PS.

Parameter	Value
c_1	13.7
c_2	50
MW_1	44 g/mol
MW_2	104.15 g/mol
ΔC_p	30.7 J/(K mol)
T_g	100.0°C

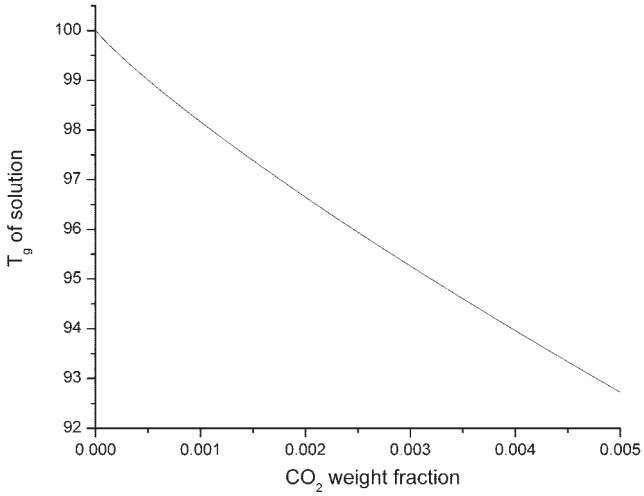

(a)

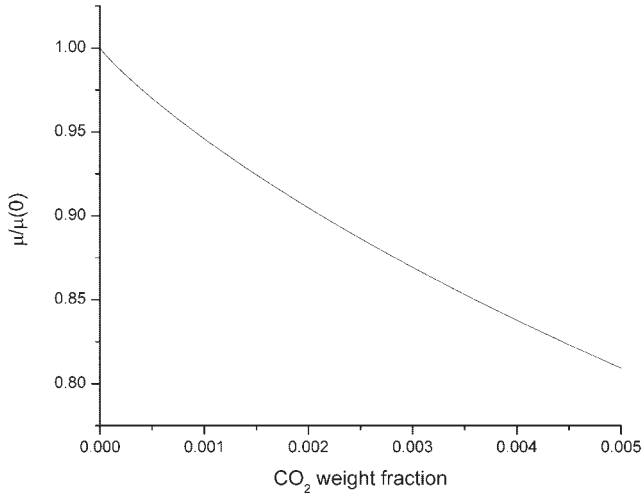

(b)

FIG. 1. Predictions of the WLF–Chow model, using the parameters of [25] for PS with CO_2. (a) Glass transition temperature T_g as a function of CO_2 concentration. (b) Viscosity as a function of CO_2 concentration.

Using a high-pressure slit-die rheometer, Royer et al. [26] measured the viscosity changes of PS with dissolved CO_2. Using the WLF equation with Chow's model, they showed that the theory successfully predicts viscosity variations with both plasticization and pressure. This is advantageous for us, since the foaming experiment of Han and Yoo [9], against which we will compare our model predictions, is also done on a PS–CO_2 system. Therefore, we will adopt the WLF–Chow parameters determined by Royer et al. [26] in our bubble-growth calculation. These are given in Table 1.

In the experiment of Han and Yoo [9], the saturation CO_2 concentration is merely 0.2 wt%. According to the predictions of the WLF–Chow model, shown in Fig. 1, this concentration produces a reduction in T_g of ~3%, and a reduction in viscosity of roughly 10%. Figure 2 compares our model predictions using a constant and a variable viscosity with the experimental data from [9]. The plasticiza-

 DOI 10.1002/pen

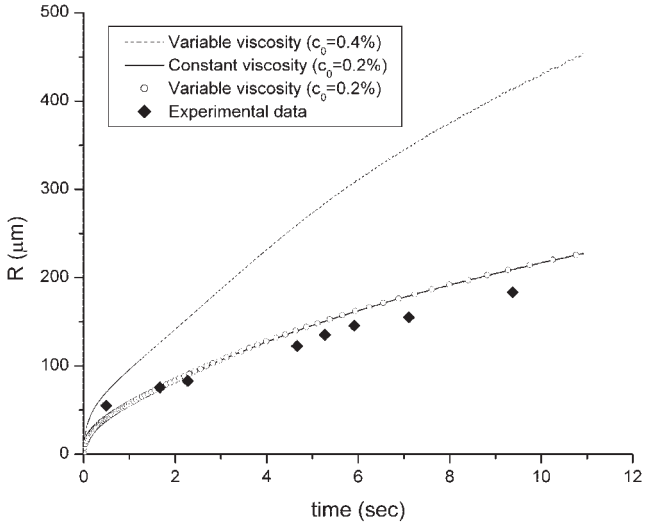

FIG. 2. Comparison between model predictions of bubble growth $R(t)$, with the experimental measurement of Han and Yoo [9]. The experimental conditions correspond to the following dimensionless parameters (constructed using pure-polymer properties): $P_a^* = 0.04605$, $Re = 1.21 \times 10^{-10}$, $Ca = 78.57$, $\beta = 0$, $k^* = 4.686$, $A^* = 2.983$, and $De = 495.0$. The solid line is computed by assuming a constant viscosity μ_0, given in [9] for the pure melt. The circles represent prediction with deplasticization with $c_0 = 0.2\%$. The dash curve is a prediction at 0.4% initial CO_2 concentration.

tion effect on bubble growth is surprisingly small in this case; the bubble radius R is only about 0.2% greater at the end of the simulation. Both predictions underpredict R at the beginning of bubble growth but overpredict it at later times.

To understand how an expected 10% viscosity reduction produces a mere 0.2% increase in bubble growth, we plot typical $c(r)$ and $\mu(r)$ profiles during bubble growth in Fig. 3. Shortly after the onset of bubble growth, a "boundary layer" forms outside the bubble in which the gas concentration drops and the viscosity recovers much of the pure-melt value. The viscosity affects the bubble growth mainly through the normal stresses τ_{rr} and $\tau_{\theta\theta}$ in *Eqs. 9* and *10*, which enter the integral in *Eq. 6*. Despite the relatively small thickness of the boundary layer, it is located next to the bubble where the normal stresses make the greatest contribution to the integral because of the $1/r$ factor. Thus, the bubble "feels" the reduced viscosity in the melt during the initial moments of growth. Afterwards, deplasticization largely restores the viscosity in the melt next to the bubble. Although the lower viscosity prevails in the plasticized melt outside the boundary layer, it imparts only a minor enhancement on the bubble growth, for the low c_0 used in [9]. Note the difference between this scenario and prior calculations for constant-viscosity fluids, e.g. Ref. 1, where the value of the viscosity does affect bubble growth strongly.

Since actual foaming operations typically use saturation concentrations much higher than $c_0 = 0.2\%$, we have also carried out numerical experiments with higher initial c_0 values. Figure 2 includes a theoretical curve with initial CO_2 concentration of 0.4%. The WLF–Chow model indicates that the initial viscosity is reduced by 17%. At the end of the simulation, the bubble radius R is roughly 100% larger than that for $c_0 = 0.2\%$. However, this increase is mostly because doubling c_0 implies doubling the amount of dissolved gas surrounding the bubble, and is equivalent to doubling the gas diffusivity. Compared with calculations at $c_0 = 0.4\%$ without plasticization, the effect due to viscosity reduction is only about 1% in this case. At a more realistic concentration of $c_0 = 10\%$, the rate of bubble growth increases more or less in proportion. However, the enhancement due to plasticization amounts to roughly 1.8%. Therefore, the variation of melt viscosity due to plasticization does not have a major effect on bubble growth, at least for PS–CO_2 systems under normal processing conditions.

In the foregoing discussion, we have neglected the effect of hydrostatic pressure, which tends to elevate T_g and counteract the effect of dissolved gas [19]. On the basis of the data in Royer et al. [26], it can be found that the rate of

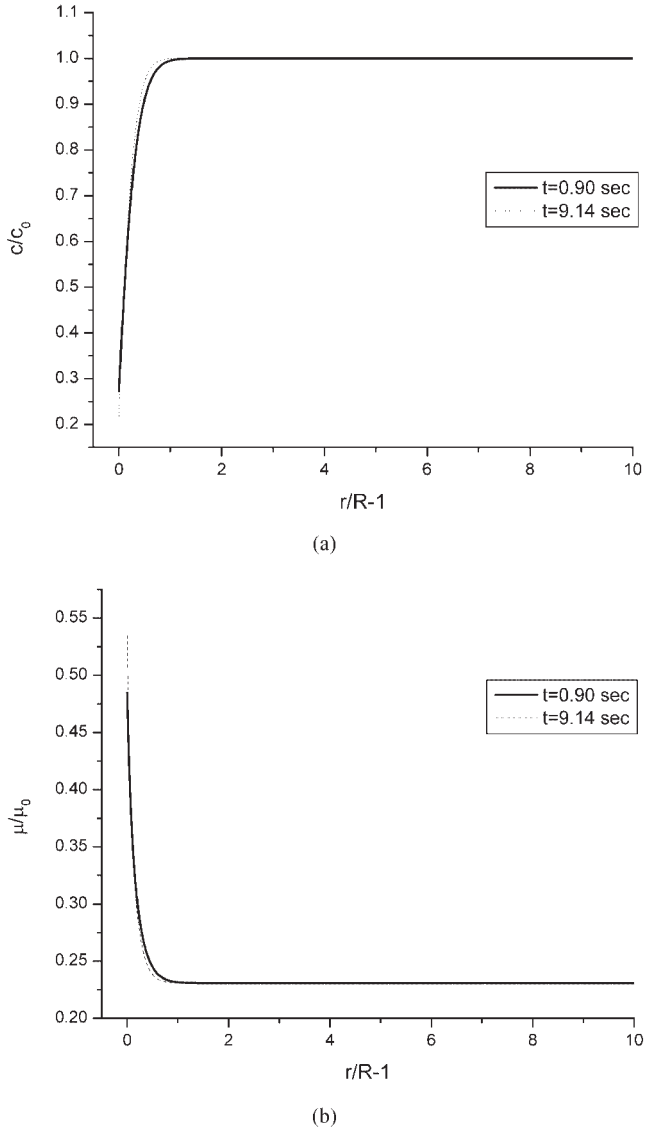

FIG. 3. Radial profiles of (a) gas concentration $c(r)$ and (b) viscosity $\mu(r)$ at different times during bubble growth. The initial concentration is $c_0 = 0.2\%$.

change for PS is roughly 0.048 K/atm. This implies an increase in T_g of up to 3°C in Han and Yoo's experiment [9], comparable to the decrease due to dissolved CO_2. Therefore, T_g probably changed little in this particular case as the two effects tend to cancel. Although this does not modify the conclusion that viscosity plasticization has little effect on bubble growth, one needs to consider the effects of solvent and pressure separately in general.

VARIABLE DIFFUSIVITY

FV Diffusion Model

Diffusion in a polymer is much more complex than diffusion in simple fluids since the polymer molecules may not remain in equilibrium conformation as they are disturbed by the solvent. For instance, the penetration of a small-molecule solvent into a bulk polymer may swell the chain network and introduce an additional stress. Such a stress enters the relaxation dynamics of the entangled chains and consequently the diffusion of the solvent [27, 28]. Under certain conditions, however, the classical Fickian diffusion theory works well for polymer melts [29–35]. These conditions have been formulated by Vrentas and Duda [32] in terms of a diffusion Deborah number.

The diffusion Debroah number (D_d) is defined by

$$D_d = \frac{\lambda_m}{\theta_D} \tag{18}$$

where λ_m and θ_D are the characteristic times of the polymer relaxation and the diffusion process [32]. If $D_d \gg 1$, the solvent molecules move in a material that appears to be an elastic solid, and the process is called elastic diffusion. If $D_d \ll 1$, on the other hand, both the polymer and the solvent behave like purely viscous liquids. For this regime of viscous diffusion, the classical Fickian theory applies. Finally, when the polymer relaxation and solvent diffusion have comparable time scales and D_d is of the order of 1, the process is known as viscoelastic diffusion. For molten polymers ($T > T_g$), Joubert et al. [35] have shown that the diffusion of a small-molecule solvent usually falls in the viscous regime. It is for glassy polymers that the diffusion-induced stress plays a significant role and non-Fickian diffusion prevails [27, 28].

In our context of polymer foaming, we will consider Fickian diffusion with the mutual diffusivity determined by a FV theory originated by Cohen and Turnbull [21] and further developed by Vrentas and Duda [30, 31]. The theory is based on the same FV ideas used in the last section to account for viscosity changes (see *Eq. 12*). Here, there are two kinds of FVs: interstitial FV and hole FV. The former relates to the molecular conformation of the polymer chain itself, while the latter occurs due to density fluctuation of the polymers [30]. The redistribution of the interstitial FV needs a large amount of energy, while the hole FV can be redistributed without changing the system's free energy. Therefore, it is reasonable to assume that the diffusion of a solvent is predominantly through hole FV. When a hole void is large enough, a nearby solvent molecule will jump into the hole if it can overcome the attraction from neighboring molecules. At high temperatures, the FV is abundant, and diffusion is mainly determined by molecular forces between the solvent and polymer molecules. If the temperature is below a threshold, typically taken to be $T_g + 100$°C, the solvent diffusion is dominated by the distribution of hole FV. Note that this is the same temperature range in which the FV theories for the viscosity apply.

In analogy to *Eq. 12*, one can write out the self-diffusivity D_1 for the solvent molecules in terms of the FVs of both components in a polymer–solvent mixture:

$$D_1 = D_{01} \exp\left(-\gamma \frac{\omega_1 \hat{V}_1^* + \xi \omega_2 \hat{V}_2^*}{\hat{V}_{FH}} \right) \tag{19}$$

where ω_1 and ω_2 are the weight fractions of the solvent and polymer (subscripts 1 and 2 will designate the two components hereafter), γ is the same overlap factor as in *Eq. 12*. $\hat{V}_1^*$ and $\hat{V}_2^*$ are the specific critical hole FV for solvent and polymer. $\hat{V}_{FH}$ is the average hole FV per gram of the mixture. The pre-exponential factor D_{01} is effectively a constant. ξ is the ratio of the critical molar volume of the solvent to that of the polymer jumping units:

$$\xi = \frac{\hat{V}_1^* M_1}{\hat{V}_2^* M_j} \tag{20}$$

where M_1 and M_j are molecular weight of the solvent and the polymer jumping unit. $\hat{V}_{FH}$ is calculated from the FV of the solvent and the polymer, using an additive rule [31, 33, 34]:

$$\frac{\hat{V}_{FH}}{\gamma} = \omega_1 \frac{K_{11}}{\gamma_1}(K_{21} + T - T_{g1}) + \omega_2 \frac{K_{12}}{\gamma_2}(K_{22} + T - T_{g2}) \tag{21}$$

where the component FV is computed from its thermal expansion coefficient. The free-volume parameters K_{11}, K_{12}, and K_{22} are related to c_1 and c_2 in the WLF equation, and will be determined from thermal variation of the component viscosities [33]. Finally, the mutual diffusivity D of the solvent can be expressed in terms of the self-diffusivity via the Flory–Huggins theory:

$$D = D_1(1 - \phi_1)^2(1 - 2\chi\phi_1) \tag{22}$$

where ϕ_1 is the solvent volume fraction and χ is the Flory–Huggins interaction parameter for the polymer/solvent pair.

DOI 10.1002/pen

Bubble Growth With Variable Gas Diffusivity

To predict the mutual diffusivity D in a polymer–solvent mixture from the FV diffusion model, one must determine some 10 model parameters. As pointed out by Vrentas and Vrentas [34], all parameters except χ can be obtained from properties of the pure components such as viscosity–temperature data. From the literature [36–39], we have compiled in Table 2 all the parameter values for a PS–CO_2 mixture.

The free-volume parameters for pure CO_2 K_{11}/γ_1 and $K_{21} - T_{g1}$ are determined from viscosity–temperature data of Xu [38], at a pressure of 1000 psi (or 6895 kPa). The pre-exponential factor D_{01} in *Eq. 20* is usually determined by fitting the diffusivity data at the limit of 0% solvent concentration [36]. In addition, Han and Yoo [9] provided a value for the mutual diffusivity $D = 5.5 \times 10^{-6}$ cm^2/s, but did not specify whether this is for the pure melt or the CO_2 saturation concentration $c_0 = 0.2\%$ in their experiment. For the theory to produce this D value at $c_0 = 0\%$ or $c_0 = 0.2\%$, we would need $D_{01} = 7.79 \times 10^{-6}$ or 1.26×10^{-6} cm^2/s, respectively. The proximity of the first value to that in Table 2 [36] might suggest that Han and Yoo's D was for pure melt. In our model calculations, however, we have tested all three values of D_{01}, and compared the results with experimental data on bubble growth. Figure 4a plots the $D(c)$ curves predicted by the FV theory, using the three D_{01} values. For the Flory–Huggins interaction parameter χ, Sheehan and Bisio [39] listed values for PS with a number of solvents, which are all close to 0.5. Figure 4b shows that D is rather insensitive to χ, especially at low gas concentration. Thus, we have used a constant $\chi = 0.5$ in our bubble-growth calculations. Note that D achieves a maximum for an intermediate c value, in agreement with experimental measurements of a large number of polymer–solvent pairs [36, 37].

Since D is very sensitive to c at low CO_2 concentrations, we expect plasticization effect on D to play a major part in bubble growth. Figure 5 partly validates this expectation. First, note that the prediction based on $D_{01} = 1.26 \times 10^{-6}$ cm^2/s (curve b) fits the experimental data fairly well. This seems to suggest that Han and Yoo's [9] value $D = 5.5 \times 10^{-6}$ cm^2/s corresponds to the mutual diffusivity at a CO_2 concentration of 0.2%. Second, the difference between curves (a) and (b) is fairly small. This is because the far-field diffusivity is the same, and (b) experiences a reduction in D only within the thin boundary layer outside the bubble (see Fig. 2a). In contrast, the difference between curve (a) and curves (c) or (d) is much larger. For the latter curves, an elevated D due to plasticization prevails through most of the melt, and produces a more rapid bubble growth. Lastochkin and Favelukis [40] have computed diffusion-controlled bubble growth, with an empirical relationship for the variable diffusivity. The enhancement in bubble growth depends strongly on an empirical parameter, and cannot be compared quantitatively with our results.

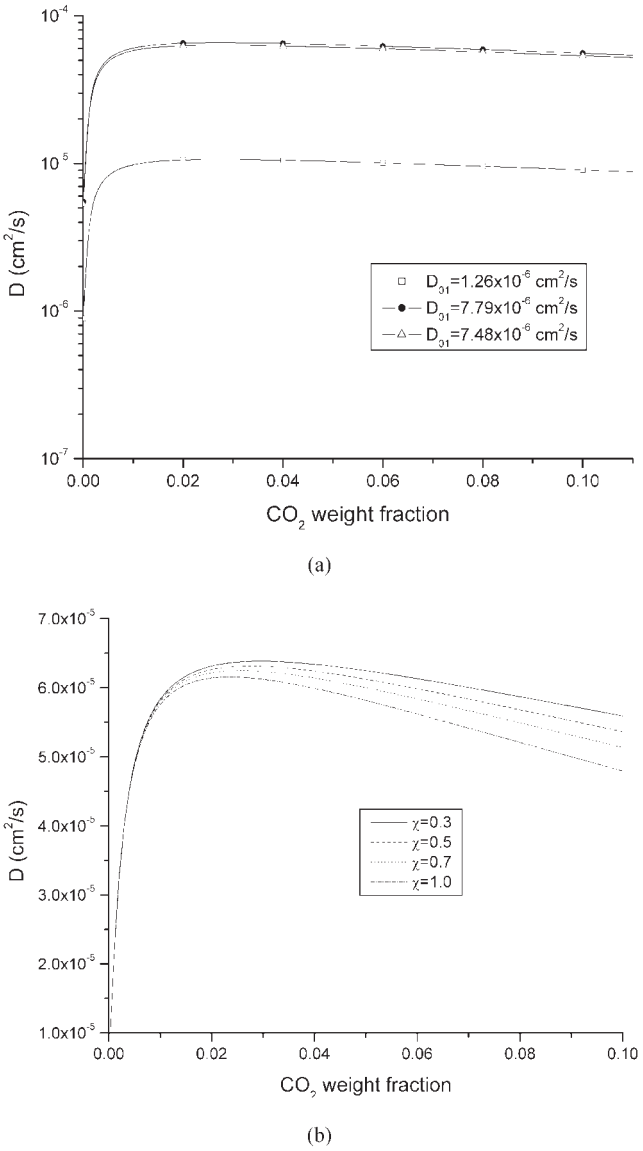

FIG. 4. Mutual diffusivity D predicted using the parameters in Table 2 with the following variations: (a) the effect of D_{01}; (b) the effect of χ.

TABLE 2. Parameters in the free-volume diffusion theory for a PS-CO_2 mixture.

Parameter	Value	Source
$\hat{V}_1^*$	0.770 cm^3/g	[36]
$\hat{V}_2^*$	0.850 cm^3/g	[37]
K_{12}/γ_2	5.39 cm^3/(g K)	[37]
$K_{22}-T_{g2}$	−323.0 K	[37]
K_{11}/γ_1	0.505 cm^3/(g K)	Fitting from [38]
$K_{21}-T_{g1}$	−293.8 K	Fitting from [38]
χ	0.5	[39]
ξ	0.252	[36]
D_{01}	7.48×10^{-5} cm^2/s	[36]

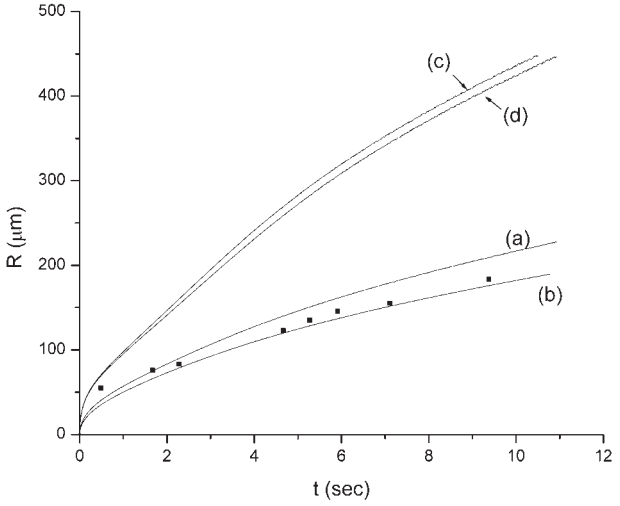

FIG. 5. Effect of plasticization-dependent gas diffusivity D on bubble growth. Experimental data of Han and Yoo [9] are also shown for comparison. The theoretical curves are (a) for a constant $D = 5.5 \times 10^{-6}$ cm^2/s, and for a variable diffusivity computed using (b) $D_{01} = 1.26 \times 10^{-6}$ cm^2/s, (c) $D_{01} = 7.79 \times 10^{-6}$ cm^2/s, and (d) $D_{01} = 7.48 \times 10^{-6}$ cm^2/s.

VARIABLE INTERFACIAL TENSION

Density Gradient Theory for Interfacial Tension

The interfacial tension σ is the areal energy density on an interface between two immiscible fluids. A popular method for calculating σ assumes a diffuse interface of a small thickness within which the fluids do mix. Then the excess free energy due to the mixing, calculable from the density profiles of the components across the interface, gives rise to σ. Sanchez [41] and Poser and Sanchez [42] developed a widely used version of the theory by combining the density gradient model of Cahn and Hilliard [43] with a lattice–fluid equation of state [44, 45]. By assuming a linear density profile in the interfacial region, Harrison et al. [46] proposed a modified expression based on Sanchez's model:

$$\sigma = \sqrt{2}\,\frac{\left|\left[\kappa_{22}^{1/2} + \kappa_{11}^{1/2}(\Delta\rho_1/\Delta\rho_2)\right]\right|}{v_{m,2}^{*}} \int_{\phi_2^{\mathrm{I}}}^{\phi_2^{\mathrm{II}}} \tilde{\rho}\Delta a^{1/2}\, d\phi_2 \qquad (23)$$

where ϕ_i ($i = 1,2$) are the volume fractions of the solvent and polymer respectively, κ_{ii} are the interaction parameters for the pure components, $\Delta\rho_i$ are the density differences of each species across the interface, with $\rho_i = \tilde{\rho}\phi_i/v_{\mathrm{m,i}}^{*}$, $\tilde{\rho}$ being the reduced density from the equation of state and $v_{\mathrm{m,i}}^{*}$ being the characteristic monomer volume defined as MW_i/ρ_i^{*} divided by the degree of polymerization. Here MW_i and ρ_i^{*} are molecular weight and close-packed mass density, respectively. Δa is the excess mixing energy defined by

$$\Delta a = \tilde{\rho}\left[g - \left(\frac{\phi_1}{v_{\mathrm{m},1}^{*}}\right)\mu_1^{\mathrm{e}} - \left(\frac{\phi_2}{v_{\mathrm{m},2}^{*}}\right)\mu_2^{\mathrm{e}} \right] \qquad (24)$$

where g is the Gibbs free energy density of a homogeneous system for a given composition within the interfacial region, and μ_i^{e} are the equilibrium chemical potentials for the two pure components, which can be determined from the lattice fluid model. The interaction parameters can be further written in terms of dimensionless reduced interaction parameters $\tilde{\kappa}_{ii}$

$$\kappa_{\mathrm{ii}} = 2P_i^{*}v_{m,1}^{*\,8/3}\tilde{\kappa}_{ii} \qquad (25)$$

where P_i^{*} is the characteristic pressure [44]. Harrison et al. [46, 47] and Li et al. [48] assumed $\tilde{\kappa}_{11} = \tilde{\kappa}_{22}$ and determined this parameter by fitting the model prediction of σ to the measured value at a certain low pressure or CO_2 concentration. All other parameter values are obtained from pure-component properties. The two groups used different $\tilde{\kappa}_{ii}$ values for their respective materials. Harrison et al. [47] showed quantitative agreement between the model prediction and experimental data. In Li et al.'s case, the agreement is qualitative, with considerable deviations. We will revisit this issue in the next subsection. In both cases, the predicted interfacial tension decreases with the amount of dissolved CO_2, consistent with the results of Lee and Flumerfelt [17] for LDPE–N_2 systems.

Bubble Growth With Variable Interfacial Tension

As we will benchmark our model prediction by the foaming experiment of Han and Yoo [9], we need the parameter values in the above theory to calculate σ for the CO_2 in PS (Styron 678 from Dow Chemical) system used in that experiment. Unfortunately, those were not given in [9]. Li et al. [48] used two kinds of PS: Nova 1037C (NOVA

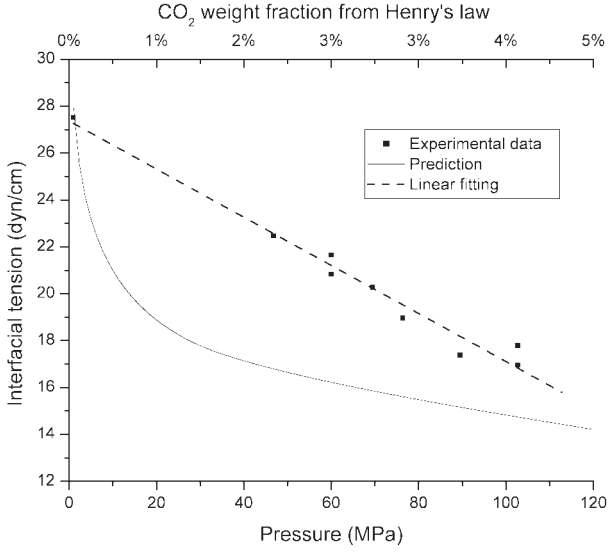

FIG. 6. Measured interfacial tension between PS and CO_2 [48] and prediction by the density gradient theory. By Henry's law, the pressure is related to CO_2 concentration in the melt by a constant coefficient given in [9].

DOI 10.1002/pen

Chemicals, MW_n = 77,100) and Styron 685D (Dow Chemical, MW_n = 120,000). The latter exhibits an interfacial tension σ = 27.7 dyn/cm at atmospheric pressure and 200°C, very close to the value 28 dyn/cm cited by Han and Yoo [9] for Styron 678. Therefore, we have adopted the fundamental parameters of Li et al. [48] in our computation.

To fit the predicted σ to the measured value at atmospheric pressure, we have chosen $\tilde{\kappa}_{ii}$ = 0.21. Figure 6 compares our theoretical prediction with the experimental data for Styron 685D from Li et al. [48]. Note that the density gradient theory naturally predicts the dependence of σ on pressure P. By Henry's law, this implies the dependence of σ on the gas concentration in the bulk of the polymer. The experimental data in Fig. 6 can be fitted to a linear σ–P relationship:

$$\sigma(\text{dyn/cm}) = 27.4 - 0.103P(\text{atm}). \quad (26)$$

The theoretical curve is highly nonlinear, however, and underestimates σ, especially for intermediate pressure value. A similar discrepancy was noted by Li et al. [48] for Nova 1037C. We believe this indicates that the theory of Sanchez and Poser [41, 42] is incomplete in some sense. According to Sanchez and Lacombe [45], the reduced interaction parameter $\tilde{\kappa}_{ii}$ is determined by the mer–mer attractive potential between parts of like molecules occupying neighboring lattice sites. Thus, it seems reasonable to expect $\tilde{\kappa}_{ii}$ to be independent of the overall size of the chain or the molecular weight. For three PS samples with increasing molecular weight, the oligmeric PS (MW_n = 1850) of [47] and Nova 1037C and Styron 685D of [48], the best-fitting $\tilde{\kappa}_{ii}$ values are: $\tilde{\kappa}_{ii}$ = 0.084, 0.5, and 0.21. This large variation suggests that the theory does not contain all the important physics of the material. In the following, we will use both the theoretical (*Eq. 23*) and experimental (*Eq. 26*) results in our bubble-growth simulation.

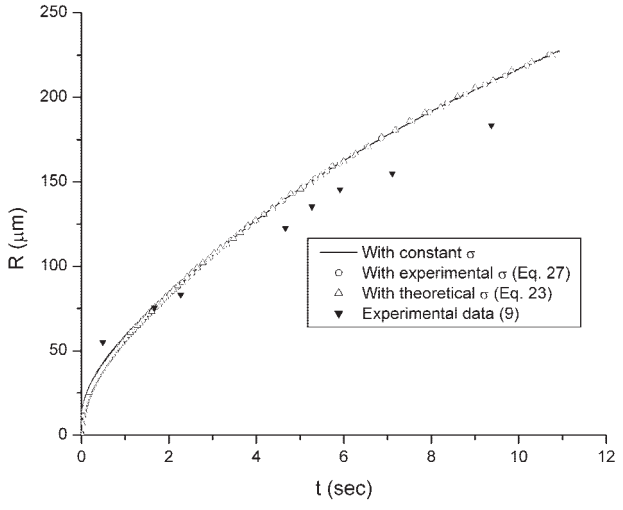

FIG. 7. Bubble growth as affected by a variable interfacial tension σ due to plasticization. For the processing condition in Han and Yoo [9], a variable σ has little effect on $R(t)$.

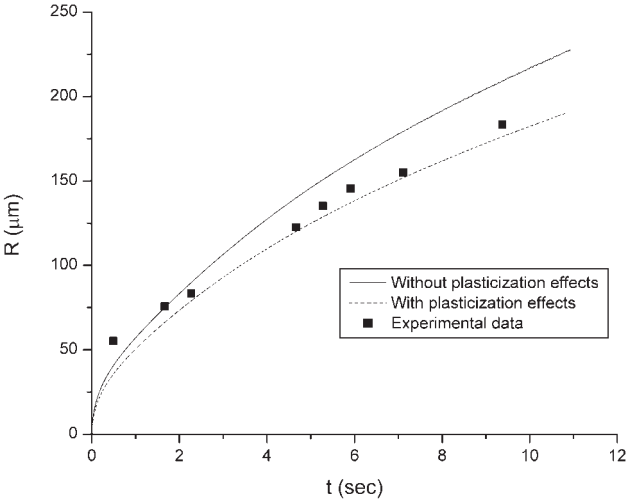

FIG. 8. Comparison between predictions with and without plasticization effects.

While the density gradient theory deals with the small length scale within the gas–polymer interface, our bubble-growth model is "coarse-grained," in the sense that it concerns macroscopic length scales with respect to which the interface is sharp. As an input to our model, σ is determined from the bubble pressure P_g (or, equivalently, from the gas concentration on the interface), which varies in time. Figure 7 plots theoretical predictions of bubble growth with a constant σ and a variable σ computed from *Eqs. 23* and *26*. The experimental data of Han and Yoo [9] are also included. The theoretical curves are almost identical, and show little effects of the variable interfacial tension. One reason for this is that Han and Yoo's experiment used a low CO_2 concentration (0.2%) and a low saturation pressure (4.6 atm), at which the plasticization effect on σ is minor. In Fig. 7, this corresponds to 18% of reduction in σ from the theoretical curve and 1.7% from the experimental correlation (*Eq. 26*). A second and more important reason for the insignificance of σ plasticization is that the capillary number $Ca = \mu D/\sigma R_0$ = 78.57 is large. From *Eq. 6*, this implies that the interfacial tension plays a very small role in bubble growth; the latter is dominated by mass diffusion and momentum balance.

As mentioned earlier, real foaming processes employ much higher blowing-agent concentrations and processing pressures than those of Han and Yoo [9]. The reduction in σ can be considerable. Lee and Flumerfelt [17] reported, for instance, a roughly 50% decrease in interfacial tension for LDPE plasticized by nitrogen, which leads to a tremendous increase in bubble nucleation rate. On the other hand, the physical parameters—melt viscosity, gas diffusivity, and interfacial tension—used in [9] and our modeling are representative of typical melts and blowing agents. Thus, we may expect the capillary number to be generally much greater than 1, and the interfacial tension σ and its plasticization to have little effect on bubble growth during foaming.

Finally, we compare model predictions with none and all three types of plasticization effects with experimental data in Fig. 8. For diffusivity, we have taken Han and Yoo's value in [9] as corresponding to the saturated melt at $c_0 = 0.2\%$, with $D_{01} = 1.26 \times 10^{-6}$ cm^2/s (see Fig. 4). Upon start of bubble growth, deplasticization causes D to drop, and the smaller D tends to suppress bubble growth. In the meantime, plasticization effects on viscosity and interfacial tension will increase bubble growth slightly. In the end, plasticization amounts to a small decrease in the rate of bubble growth in this case, and brings the theoretical prediction into better agreement with experimental data.

CONCLUSIONS

Plasticization and deplasticization play important roles in foaming of plastics through changes in the viscosity, solvent diffusivity, and gas–melt interfacial tension. Various theories have been proposed for these changes, including FV theories for the plasticization effects on the viscosity and diffusivity and the density gradient theory for the interfacial tension. This paper strives to incorporate these theories into a model for diffusion-driven bubble growth, and to explore the effects of plasticization under conditions for a foaming experiment in a PS–CO_2 system.

Our results show that the increase of blowing-agent diffusivity due to plasticization can greatly boost the rate of bubble growth, even at relatively low gas concentration. In contrast, plasticization-induced variations in the melt viscosity and interfacial tension have little effect on bubble growth. These conclusions are expected to hold for typical foaming conditions and common polymer-blowing agent combinations.

To some extent, this work is handicapped by the lack of pertinent experimental data for comparison. Plasticization and deplasticization occur naturally during foaming. To quantify their effects, one would have to run control experiments that are free from plasticization, which is difficult if at all possible. In lack of such direct comparison, we have established the plasticization effects by studying model parameters that are correlated to experiments. In this connection, we also note the scarcity of reliable data, for example on diffusivity [7], and the need to further test the conclusion of this work as more data become available. As far as we are aware, the only prior modeling of plasticization during bubble growth is by Ramesh and Malwitz [16] and Lastochkin and Favelukis [40]. They showed that using a viscosity and a diffusivity that depend on the blowing-agent concentration greatly improves the prediction of their model. This is consistent with our findings.

ACKNOWLEDGMENTS

We thank Professor David Tomasko of the Ohio State University for useful discussions.

REFERENCES

1. M. Amon and C.D. Denson, *Polym. Eng. Sci.*, **24**, 1026 (1984).
2. A. Arefmanesh and S.G. Advani, *Rheol. Acta*, **30**, 274 (1991).
3. N.S. Ramesh, D.H. Rasmussen, and G.A. Campbell, *Polym. Eng. Sci.*, **31**, 1657 (1991).
4. M.A. Shafi, K. Joshi, and R.W. Flumerfelt, *Chem. Eng. Sci.*, **52**, 635 (1997).
5. K. Joshi, J.G. Lee, M.A. Shafi, and R.W. Flumerfelt, *J. Appl. Polym. Sci.*, **67**, 1353 (1998).
6. D.C. Venerus and N. Yala, *AIChE J.*, **43**, 2948 (1997).
7. D.C. Venerus, N. Yala, and B. Bernstein, *J. Non-Newtonian Fluid Mech.*, **75**, 55 (1998).
8. J.J. Feng and C.A. Bertelo, *J. Rheol.*, **48**, 439 (2004).
9. C.D. Han and H.J. Yoo, *Polym. Eng. Sci.*, **21**, 518 (1981).
10. C.B. Park, L.K. Cheung, and S.W. Song, *Cell. Polym.*, **17**, 221 (1998).
11. J. Sandler, F. Wollecke, V. Altsadt, E. Wettstein, and D. Rakutt, *Cell. Polym.*, **19**, 371 (2000).
12. J. Tatibouet, J.R. Gendron, A. Hamel, and A. Sahnoune, *J. Cell. Plast.*, **38**, 203 (2002).
13. D. Klempner and K.C. Frisch, *Handbook of Polymer Foams and Foam Technology*, Hanser, New York (1991).
14. S.-T. Lee, *Foam Extrusion*, Technomic, Lancaster, PA (2000).
15. R. Gendron and L.E. Daigneault, L.M. Caron, *J. Cell. Plast.*, **35**, 221 (1999).
16. N.S. Ramesh and N. Malwitz, *J. Cell. Plast.*, **35**, 199 (1999).
17. J.G. Lee and R.W. Flumerfelt, *J. Colloid Interface Sci.*, **184**, 335 (1996).
18. M. Schnell and B.A. Wolf, *Polymer*, **42**, 8599 (2001).
19. J.D. Ferry, *Viscoelastic Properties of Polymers*, 2nd ed., Wiley, New York (1970).
20. A.K. Doolittle, *J. Appl. Phys.*, **22**, 1471 (1951).
21. M.H. Cohen and D. Turnbull, *J. Chem. Phys.*, **31**, 1164 (1959).
22. T.S. Chow, *Macromolecules*, **13**, 362 (1980).
23. D.L. Tomasko, H. Li, D. Liu, X.M. Han, M.J. Wingert, L.J. Lee, and K.W. Koelling, *Ind. Eng. Chem. Res.*, **42**, 6431 (2003).
24. L.J. Gerhardt, C.W. Manke, and E. Gulari, *J. Polym. Sci. Part B: Polym. Phys.*, **35**, 523 (1997).
25. C. Kwag, C.W. Manke, and E. Gulari, *J. Polym. Sci. Part B: Polym Phys.*, **37**, 2771 (1999).
26. J.R. Royer, Y.J. Gay, J.M. Desimone, and S.A. Khan, *J. Polym. Sci. Part B: Polym Phys.*, **38**, 3168 (2000).
27. D.A. Edward, *Z. Angew. Math. Phys.*, **52**, 254 (2001).
28. D.G. Bucknall, *Prog. Mater. Sci.*, **49**, 713 (2004).
29. R.J. Bearman, *J. Phys. Chem.*, **65**, 1961 (1961).
30. J.S. Vrentas and J.L. Duda, *J. Polym. Sci. Polym. Phys. Ed.*, **15**, 403 (1977).
31. J.S. Vrentas and J.L. Duda, *J. Polym. Sci. Polym. Phys. Ed.*, **15**, 417 (1977).
32. J.S. Vrentas and J.L. Duda, *J. Polym. Sci. Polym. Phys. Ed.*, **15**, 441 (1977).
33. S.U. Hong, *Ind. Eng. Chem. Res.*, **34**, 2536 (1995).

 DOI 10.1002/pen

34. J.S. Vrentas and C.M. Vrentas, *Eur. Polym. J.*, **34**, 797 (1998).
35. C. Joubert, P. Cassagnau, L. Choplin, and A. Michel, *J. Rheol.*, **46**, 629 (2002).
36. J.S. Vrentas and J.L. Duda, *J. Appl. Polym. Sci.*, **21**, 1715 (1977).
37. J.S. Vrentas and J.L. Duda, *Macromolecules*, **27**, 4684 (1994).
38. J. Xu, *Carbon Dioxide Thickening Agents for Reduced CO_2 Mobility*, Ph.D. Dissertation, University of Pittsburgh (2003).
39. C.J. Sheehan and A.L. Bisio, *Rubber Chem. Technol.*, **39**, 149 (1966).
40. D. Lastochkin and M. Favelukis, *Chem. Eng. J.*, **69**, 21 (1998).
41. I.C. Sanchez, *J. Macromol. Sci. Phys. B*, **17**, 565 (1980).
42. C.I. Poser and I.C. Sanchez, *Macromolecules*, **14**, 361 (1981).
43. J.W. Cahn and J.E. Hilliard, *J. Chem. Phys.*, **28**, 258 (1958).
44. R.H. Lacombe and I.C. Sanchez, *J. Phys. Chem.*, **80**, 2568 (1976).
45. I.C. Sanchez and R.H. Lacombe, *Macromolecules*, **11**, 1145 (1978).
46. K.L. Harrison, K.P. Johnston, and I.C. Sanchez, *Langmuir*, **12**, 2637 (1996).
47. K.L. Harrison, S.R.P. da Rocha, M.Z. Yates, K.P. Johnston, D. Canelas, and J.M. DeSimone, *Langmuir*, **14**, 6855 (1998).
48. H. Li, L. J. Lee, and D.L. Tomasko, *Ind. Eng. Chem. Res.*, **43**, 509 (2004).